HHS Public Access

Author manuscript

Cell Rep. Author manuscript; available in PMC 2021 April 29.

Published in final edited form as:

Cell Rep. 2021 April 06; 35(1): 108934. doi:10.1016/j.celrep.2021.108934.

Slower prefrontal metastable dynamics during deliberation predicts error trials in a distance discrimination task

Danilo Benozzo[1], **Giancarlo La Camera**[2,3,*], **Aldo Genovesio**[1,3,4,*]

[1]Department of Physiology and Pharmacology, Sapienza University of Rome, Rome, Italy

[2]Department of Neurobiology and Behavior, Center for Neural Circuit Dynamics and Institute for Advanced Computational Science, State University of New York at Stony Brook, Stony Brook, NY, USA

[3]Senior author

[4]Lead contact

SUMMARY

Cortical activity related to erroneous behavior in discrimination or decision-making tasks is rarely analyzed, yet it can help clarify which computations are essential during a specific task. Here, we use a hidden Markov model (HMM) to perform a trial-by-trial analysis of the ensemble activity of dorsolateral prefrontal cortex (PFdl) neurons of rhesus monkeys performing a distance discrimination task. By segmenting the neural activity into sequences of metastable states, HMM allows us to uncover modulations of the neural dynamics related to internal computations. We find that metastable dynamics slow down during error trials, while state transitions at a pivotal point during the trial take longer in difficult correct trials. Both these phenomena occur during the decision interval, with errors occurring in both easy and difficult trials. Our results provide further support for the emerging role of metastable cortical dynamics in mediating complex cognitive functions and behavior.

In brief

Benozzo et al. analyze the neural activity in the prefrontal cortex of rhesus monkeys performing a distance discrimination task. The neural activity is a sequence of metastable states. State durations are longer before errors and at the beginning of the deliberation period in trials characterized by correct difficult discriminations.

Graphical Abstract

*Correspondence: giancarlo.lacamera@stonybrook.edu (G.L.C.), aldo.genovesio@uniroma1.it (A.G.).

AUTHOR CONTRIBUTIONS

A.G. designed the experimental task and collected the data. D.B., G.L.C., and A.G. designed the data analysis and wrote the paper. D.B. performed research. G.L.C. and A.G. supervised research.

DECLARATION OF INTERESTS

The authors declare no competing interests.

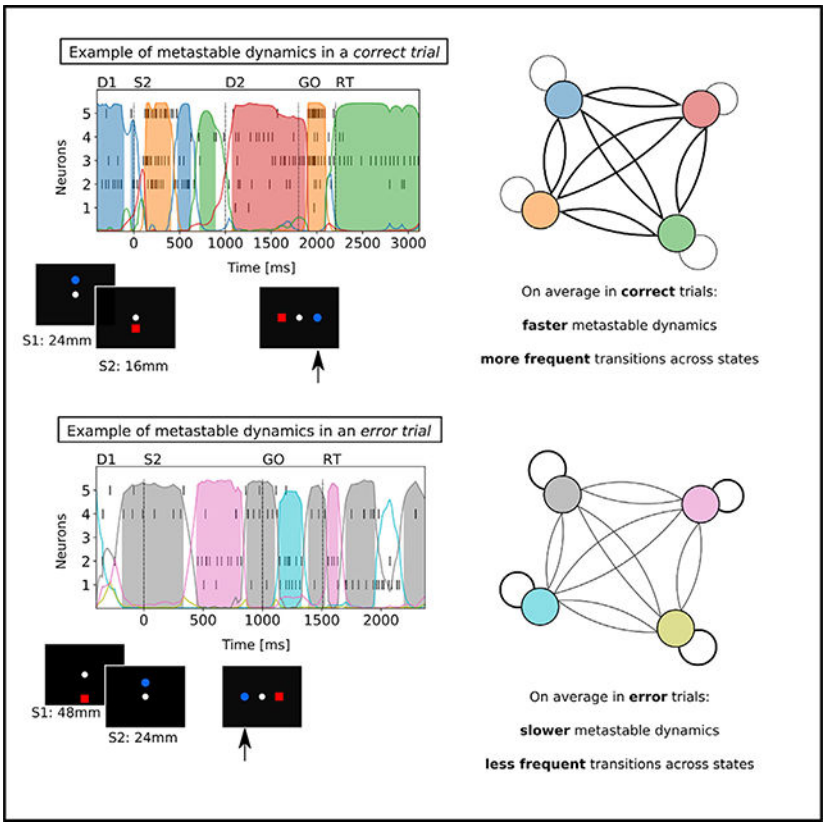

INTRODUCTION

The role of the prefrontal cortex in decision making has been demonstrated using a variety of tasks (Kim and Shadlen, 1999; Hoshi et al., 2000; Freedman et al., 2001; Tanji and Hoshi, 2001; Genovesio et al., 2012; Maoz et al., 2013; Marcos and Genovesio, 2016; Rich et al., 2018), including tasks with decisions in the temporal (Genovesio et al., 2009) and spatial (Genovesio et al., 2011) domains. In particular, we have shown previously that prefrontal neurons encode the decision about which stimulus was presented farther from the center in a distance discrimination task (Genovesio et al., 2011), as well as the transformation of goals into action (Marcos et al., 2019). Prefrontal neurons also code for the duration and distance magnitude to be maintained in working memory, using domain-specific representations of distance and duration in dorsolateral prefrontal cortex (PFdl) neurons (Marcos et al., 2017). However, in the spatial discrimination task, the effect of trial difficulty has not been addressed, and previous analyses could not unmask which type of failure could account for the response errors. It is possible that such information could be found in the collective activity of ensembles of neurons. For example, ensembles of monkey premotor neurons transition more quickly to a new state in easier trials during a vibro-tactile discrimination task (Ponce-Alvarez et al., 2012). One might also suspect that ensemble activity is related to behavioral performance and not just trial difficulty. Little is known, however, about the substrate of behavioral errors in terms of collective activity of ensembles of neurons. Examining collective neural activity during errors might also help us to understand what

generates the switch in coding from correct to erroneous decisions observed at the level of single neurons (Genovesio et al., 2011). A particularly promising approach in investigating the relationship between decision processes and ensemble neural activity is the use of a hidden Markov model (HMM) to segment the neural activity into sequences of discrete, metastable states. In its more frequent applications to neural data so far (Abeles et al., 1995; Jones et al., 2007; Kemere et al., 2008; Ponce Alvarez et al., 2008, 2012; Mazzucato et al., 2015; Engel et al., 2016; Sadacca et al., 2016; Linderman et al., 2016), the HMM assumes that the neural dynamics proceeds as a sequence of hidden states, wherein each state is a collection of firing rates across simultaneously recorded neurons. Reliable sequences of HMM states have been found in frontal (Abeles et al., 1995), gustatory (Jones et al., 2007; Mazzucato et al., 2015), premotor, and motor areas (Ponce-Alvarez et al., 2012) of primates and rodents in the context of different tasks. State sequences also seem to underlie internal states of attention (Engel et al., 2016), expectation (Mazzucato et al., 2019), and deliberation during decisions (Rich and Wallis, 2016). In this work, we investigate the nature of neural ensemble dynamics in the PFdl of monkeys performing the distance discrimination task of Genovesio et al. (2011, 2012). In this task, the monkeys were required to choose which of two stimuli sequentially presented was farther from the center of a computer screen (Figure 1). We focused on two main questions: whether the neural activity in PFdl could be characterized as metastable and, if so, what the links are among metastable state durations, state transition times, trial difficulty, and task performance (correct versus incorrect trials). We found that PFdl activity can be characterized as a sequence of metastable states, some of which code for the relative distance of the two stimuli from the center, based on stimulus features or order of presentation. Most notably, however, we found that the mean duration of metastable states was longer before errors. Thus, a slowdown of the metastable dynamics after the presentation of the second stimulus (S2) was typically associated with an incorrect response. We also found a link between trial difficulty and hidden state transitions in correct trials (Ponce-Alvarez et al., 2012). Specifically, the first state transition after S2 was faster in easier trials, even though the reaction times (RTs) were not different. This suggests that transition times reflect the level of trial difficulty, even when the delay before a response is too long to affect the RT. Overall, these results show a potential role of metastable dynamics in PFdl neurons during a decision process in the spatial domain, adding to accumulating evidence for a role of metastable dynamics in neural coding and cognition (La Camera et al., 2019).

RESULTS

Metastability of prefrontal neural activity during distance discrimination

To find neural correlates of behavior in the ensemble dynamics, we first characterized the dynamics by performing an HMM analysis of the ensemble activity of correct and error trials (see Figure 2 and STAR Methods for details of the procedure). We found that ensemble neural activity was well described by sequences of metastable states, in which each state was defined as a collection of firing rates across simultaneously recorded neurons, with the number of states varying between 2 and 5 across sessions. As in previous accounts (Abeles et al., 1995; Jones et al., 2007; Mazzucato et al., 2015, 2019; Ponce-Alvarez et al., 2012), state transitions varied trial by trial and were not necessarily locked to external

relevant events. This can be illustrated by warping time so that events in different trials occur simultaneously (Recanatesi et al., 2020), while onset and offset times of states are variable, as indicated in Figure 3A for an illustrative session (see STAR Methods for details). From this plot, it is apparent that the blue state tends to occur after S2 and the GO signal, whereas the yellow state tends to occur after the decision (RT). However, the time at which transitions occur varies from trial to trial, as documented in the aforementioned studies. Moreover, during trial epochs in which no clear external events occur, such as halfway after S2 and during the delay period, state transitions are much more variable, possibly reflecting the internal dynamics of state deliberation (this is discussed later).

The orderly sequences observed in Figure 3A were not an artifact of the HMM analysis, as they disappear in shuffled datasets. We used two types of shuffling procedures introduced by Maboudi et al. (2018), which we call circular and swap shuffles (see STAR Methods). As indicated in Figures 3B and 3C, both shuffling procedures disrupted the temporal alignment between state sequence and task events. The difference with the original data is especially evident after S2, the GO signal, and RT. Moreover, model selection had a larger score (smaller Bayesian information criterion; BIC) in the original data than in the shuffled datasets (Figure 3D), revealing worse HMM fits when the data were shuffled. The analysis also shows a significant reduction of the optimal number of states after swap-shuffling the data (between 2 and 3 compared to 2–5, with a median of 3 for the original data; Figure 3E). The comparison with shuffled datasets shows that the presence of metastable activity and the potential meaning of hidden states are not artifacts of the HMM analysis.

To investigate how the hidden states relate to relevant task variables, we searched for “coding states.” We define a coding state as a hidden state that tends to recur significantly more often in a specific task condition compared to other task conditions (Mazzucato et al., 2019). To illustrate this notion, in Figures 3A–3C, trials were grouped according to the features (blue circles versus red squares) of the farther stimulus from the center. The separation between the two groups is indicated by the black horizontal line, with extremities marked by triangles. Note that, during S2 and before D2, the yellow state appears only in trials that are above the horizontal separation line, and, therefore, it is a coding state for relative distance based on stimulus features (i.e., “red farther” or “blue closer”) in the current trial ($p < 0.05$, χ^2 test; see STAR Methods for details). We found coding states for the features of the farther stimulus in 22% of the sessions (two example sessions are indicated in Figure 4A). This is a significantly larger fraction than the 6% found in the circularly shuffled datasets ($p = 0.0006$, χ^2 test; not enough state transitions occurred in the swap-shuffled data). We also found evidence for coding states for relative distance based on the order of presentation (“S2 farther or closer from the center”) in 19% of sessions (two example sessions are indicated in Figure 4B). For comparison, only 5% of sessions in shuffled datasets had coding states for relative distance based on the order of presentation, a significant difference ($p = 0.002$, χ^2 test). We did not find coding states significantly associated with target position (left versus right) between the GO signal and RT (6% of sessions versus 2% of shuffled sessions; $p = 0.089$, χ^2 test). This set of comparisons with shuffled datasets shows that the presence of metastable activity, as well as the nature of hidden states as coding for relevant task variables, is not an artifact of the HMM analysis.

Mean state durations predict incorrect trials

As indicated in Figure 5A, RTs were longer in error trials than in correct trials. However, RTs were neither correlated with task difficulty (Jonckheere's trend test, p = 0.10) nor correlated with the time of first transition after S2 (Spearman's rank correlation, $r = 0.05$, p = 0.31; see the next section for details). Based on recent findings on the role of metastable dynamics in cognitive processes (Mazzucato et al., 2019), we considered the possibility that longer RTs in error trials may result from a global modulation of the neural dynamics. For example, a slowdown of the dynamics would manifest itself through longer state durations and, therefore, less frequent transitions among hidden states. To test this hypothesis, we compared the mean durations of the hidden states in both conditions (correct versus error) over a time interval going from 400 ms before S2 onset until the end of the trial (Figure 5B). In analyzing state durations, only states occurring after S2 were considered. Based on the criteria reported in STAR Methods, we analyzed 56 sessions. On average, there were 82 ± 35 correct trials and 22 ± 11 incorrect trials per session (mean ± SD). The optimal number of states of the HMM in each session ranged from 2 to 5 across sessions, with a median of 3 for both correct and incorrect trials. We found that the mean state duration after S2 was significantly greater in incorrect trials, 374.0 ± 9.4 ms (mean ± SEM), than in correct trials, 321.8 ± 3.7 ms ($p < 0.001$, two-sided Mann-Whitney U test; Figure 5B).

A longer state duration in incorrect trials is in line with the hypothesis that the slower RTs in incorrect trials are associated with a global slowdown of the dynamics. However, we found only a negligible correlation between mean state durations after the GO signal and RTs (Spearman's rank correlation, $r = 0.05$ for correct trials, p = 0.0009; and $r = -0.01$ for error trials, p = 0.75). It is possible that cortical slowdown occurs during the deliberation period only and that it directly affects the decision but not the RT (which occurs after the GO signal).

To test this hypothesis, we computed the mean state durations in two periods, from S2 to GO (deliberation period) and from GO to the end of the trial (included the intertrial interval), and performed a two-way ANOVA, with trial type (correct/incorrect) and temporal window as factors (Figure 5C). Both the main effects of trial type and temporal window were significant ($p < 0.001$): overall, state durations were longer during the S2-GO period compared to the GO-END period (in both correct and incorrect trials; see Figures 5D and 5E for the distributions of mean state durations). However, the reduction in mean state duration observed in the GO-END period (compared to the S2-GO period) was larger in error trials compared to that in correct trials (Figure 5C; p (interaction) $<10^{-5}$, $F(1) = 16.3$; Figures 5D and 5E show distributions of mean state durations in the two time periods, together with examples from single sessions). This result shows that slowing down of cortical dynamics occurred mostly in the S2-GO period, i.e., in the period when internal deliberation occurs (360 ms in correct trials versus 440 ms in error trials). After the GO signal, state durations dropped below 300 ms in both correct and incorrect trials, suggesting that cortical slowdown occurred during deliberation rather than during the motor action (accordingly, state durations after GO were not correlated with trial difficulty, i.e., with |S2–S1|: Jonckheere's trend test gave p = 0.06 for error trials and p = 0.21 for correct trials). The difference in state durations was also reflected in the HMM, specifically in the distributions of self-transition rates, λ_{ii}

(the diagonal elements of the transition matrix of the HMM), which were significantly larger in error trials than in correct trials ($p = 0.002$, Kolmogorov-Smirnov test).

We validated this result by repeating the HMM analysis with a balanced number of correct and error trials within each session. Since error trials were always fewer than correct trials, a random subsample of correct trials was selected in each session, and the procedure was repeated 20 times. During the deliberation period (S2-GO), we found longer state durations in error trials in 19 out of 20 subsampling repetitions ($p < 0.001$, Wilcoxon signed-rank test). As a control, we also performed the same analysis after shuffling the data (circular and swap shuffle; see STAR Methods and Figure 3). When the data were circularly shuffled, the mean state duration in error trials was found to be longer than in correct trials in about half of the shuffled dataset (11 out of 20), while it was found to be shorter in the other half ($p = 0.39$, Wilcoxon signed-rank test), consistent with the null hypothesis of no difference in state durations between correct and error trials. The ratio 19/20 is significantly larger than the ratio 11/20 obtained in the shuffled data ($p = 0.0035$, χ^2 test for proportions), suggesting that our result is a true property of the data. In the swap-shuffled data, we mostly found 2 states (Figure 3E), which resulted in only a handful of trials with at least 2 transitions in each session, precluding a meaningful analysis of the state durations in this case.

To further quantify the link between mean state durations and performance, we decoded the monkey performance in a fictitious 2AFC task in which we were presented with a correct and an error trial, and for each such pair, we predicted that the error trial is the one with longer mean state duration (see STAR Methods for details). This analysis was performed in 35 of 56 sessions with significantly longer state durations in the S2-GO period during error trials, and it correctly predicted the performance in (72% ± 16%) of the trials (area under the receiver operating characteristic [ROC] curve, mean ± SD). A similar analysis using RTs rather than state durations gave similar results, (72% ± 12%). On a trial-by-trial basis, state durations or RTs would predict the behavior of the monkey in 72% of the trials, and although this is not remarkable in terms of predictive performance, it is well above chance level ($p < 0.001$ in a 2AFC task with $n \geq 46$ trials, binomial test). Finally, we also found that we could decode the trial type by comparing the posterior probabilities based on the HMM for correct and error trials, respectively. Specifically, we classified a trial as correct if its posterior under the HMM for correct trials was larger than under the HMM for error trials, and we classified the trial as an error trial otherwise, obtaining a balanced accuracy (see STAR Methods) of 79%.

Neural correlates of trial difficulty

After examining the relationship between neural dynamics and performance, we examined the effect of trial difficulty on metastable dynamics. Despite a non-significant trend before the GO signal (data not shown), average state duration was not correlated with trial difficulty (between S2 and GO: $p = 0.059$, Jonckheere's trend test; linear regression slope = −1.25, $p = 0.24$; after GO: $p = 0.28$, Jonckheere's trend test; linear regression slope = −0.22, $p = 0.70$). In search for a more significant neural correlate of trial difficulty, we followed Ponce-Alvarez et al. (2012) study and looked at the first transition to a new state after S2 onset (fTaS2). The hypothesis was that, regardless of mean state durations, transitions after S2

onset would occur sooner in easy trials than in difficult trials. Figure 6 indicates two examples of HMM analysis for one difficult trial (Figure 6A) and one easy trial (Figure 6C). The HMM was first performed with only 2 states and centered on a 1,400-ms window around S2—specifically, from 400 ms before to 1,000 ms after S2 offset—and during correct trials only. To increase statistical power, the HMM analysis was performed separately on trials with S2 appearing above the central stimulus and on trials with S2 appearing below the central stimulus (however, an HMM with all trials lumped together gave similar results; this is discussed in the subsequent text). Sessions were then selected based on the ability of the HMM to decode the monkeys' decision (see STAR Methods). Only sessions with a significant decoding performance were kept for further analysis: 41/61 sessions with S2 appearing above the central stimulus and 34/61 sessions with S2 appearing below, comprising, on average, 27.6 ± 12.8 trials per session (mean ± SD). Decoding performance was significantly better than in shuffled datasets, where the same analysis was performed after randomly shuffling the class labels (S1 > S2 versus S2 > S1; see STAR Methods). In this case, the decoding performance was significant only in 7/61 sessions (S2 above the stimulus, $p < 3\times10^{-10}$, χ^2 test) and in 6/61 sessions (S2 below the stimulus, $p < 7\times10^{-8}$, χ^2 test). As hypothesized, the first transition time after S2 correlated with trial difficulty, with faster transitions occurring in easier trials (Figure 6E). Specifically, we divided all trials in 5 groups according to the difference in spatial distance between S1 and S2 and found a significant decreasing trend of fTaS2 with increasing |S2–S1| (p = 0.006, Jonckheere's trend test) (Bewick et al., 2004). Slope of linear regression fit = −1.74 (p = 0.015, two-sided Wald test with t distribution; an HMM with S2 appearing both above and below the central stimulus gave similar results: linear regression slope = −1.058, p = 0.015). This trend disappeared when the data were shuffled (data not shown; p = 0.28 for circular shuffle, and p = 0.46 for swap shuffle, respectively; Jonckheere's trend test).

These results mirror previous results in motor and dorsal premotor cortex of monkeys (Ponce-Alvarez et al., 2012) and suggest that the signature of a longer process of deliberation in PFdl neurons is a longer transition out of the state present at S2 onset. Since spatial target selection and actions occur after the GO signal, when, presumably, the decision process has already occurred (except, perhaps, in some of the very difficult trials), faster transition times after S2 would not be expected necessarily to correlate with faster RTs (the time from GO to action). Indeed, we found that fTaS2s and RTs were uncorrelated (Spearman's rank correlation, $r = 0.05$, p = 0.31). In keeping with this interpretation, we performed a similar analysis for the transition time after GO (Figures 6B–6D) and found no relationship with trial difficulty (p = 0.06, Jonckheere's trend test; Figure 6F). In this case, the HMM analysis was performed in a time interval of −400 ms and +1,000 ms around the GO signal. Similarly, the RTs (time between GO and action) did not depend on trial difficulty (p = 0.10, Jonckheere's trend test; Figure 6G).

DISCUSSION

Metastable dynamics of cortical circuits is emerging as a flexible framework to interpret an increasing number of neural phenomena and related behaviors, including working memory (Abeles et al., 1995; Ponce-Alvarez et al., 2012), selective attention (Engel et al., 2016), and decision tasks (Rich and Wallis, 2016) in monkeys; navigation (Maboudi et al., 2018),

expectation (Mazzucato et al., 2019), and decision tasks (Miller and Katz, 2010) in rodents; and even task-related information in human decision making (Taghia et al., 2018; see La Camera et al., 2019, for a recent review).

Here, we found that the neural activity of ensembles of PFdl neurons of monkeys performing a distance discrimination task are well described as sequences of metastable states. Among those states, some specifically code for the relative distance of the two stimuli from the center, based on stimulus features or order of presentation. Most importantly, this study has uncovered a new role of discrete-state metastable dynamics in the PFdl neurons of monkeys performing a distance discrimination task. Our main results suggest that (1) incorrect decisions correspond to a slowing down of the metastable dynamics preceding the action, regardless of trial difficulty; and (2) a slower state transition after S2 occurs in difficult correct trials, compared to a faster transition in easy correct trials. We begin by discussing the latter.

Effect of task difficulty on state transitions

Single units in the PFdl neurons contain information about the decision on which stimulus is farther from the central stimulus (Genovesio et al., 2011). Whether they also encode trial difficulty is not clear. Based on previous studies in primary motor and premotor cortex (Pardo-Vazquez et al., 2008; Ponce-Alvarez et al., 2012) and prefrontal cortex (Kim and Shadlen, 1999), we expected PFdl neuron activity to be affected by trial difficulty. We followed Ponce-Alvarez et al. (2012) and looked for this information in the ensemble dynamics of PFdl neurons as modeled by HMM. We found that, in difficult trials, the state transition after S2, but not the GO signal, had a later onset compared to that in easier trials. Thus, the state transition latency reflected trial difficulty only in the deliberation period and not later during the transformation from goal to action. This may also explain why, although slower in error trials, RTs were not correlated with trial difficulty.

Our results are analogous to those found by Ponce-Alvarez et al. (2012) in motor and dorsal premotor cortex of monkeys engaged in a delayed vibro-tactile discrimination task. Our findings are also somewhat reminiscent of results obtained in rat gustatory cortex in very different contexts. Specifically, Moran and Katz (2014) found that the transition among 2 HMM states evoked by sucrose were delayed by conditional taste aversion, while Mazzucato et al. (2019) found a faster onset of certain hidden states (named “coding states”) when a stimulus was expected, compared to the case where it was not expected. We will say more on this later.

Slowdown of metastable dynamics in error trials

The other main result of this study is the link between a modulation of metastable activity and behavior. Specifically, we found an increased duration of hidden states during error trials compared to correct trials. Moreover, this occurred during the deliberation period and not after the GO signal prompting the behavioral response. This result indicates that, during errors, one critical aspect that can be affected is the passage through states that presumably characterize different phases of the task, and before the action takes place. We are confident that the affected period reflects an internal deliberation, because, in our task, the targets’

positions are revealed only at the GO signal, separating in time the deliberation phase from target selection and movement preparation.

Similarly, we found that RTs were related to performance (correct versus error) and not "objective" trial difficulty (where the latter is defined based on the relative distance between the two stimuli). It seems, therefore, that the RTs also reflected the internal process of deliberation and whether such process resulted in correct performance, regardless of objective trial difficulty. These findings are reminiscent of intriguing results obtained in the orbitofrontal cortex by Rich and Wallis (2016), who showed that slow deliberation was related to equal times spent in the latent states representing the available targets during a choice, rather than the difficulty of the decision as judged by eye movements. The closest analogy, however, is with the study of Mazzucato et al. (2019), who found shorter state durations when a stimulus was expected, compared to the case where it was not expected. The comparison with Mazzucato et al. (2019) invites speculation that correct decisions are more likely in trials in which expectations are successfully formed because, based on that study, this would predict faster dynamics in correct trials compared to error trials, as found here. In Mazzucato et al. (2019), faster neural dynamics was related to faster stimulus decoding, not behavioral performance. The link with behavior was provided via a spiking network model, which showed that distractor stimuli could induce the opposite effect of slowing down the dynamics. If distractors would be more likely to induce an error, this would again predict slower dynamics before errors. Here, we provide direct experimental evidence of a slowdown of the cortical dynamics during errors. To our knowledge, this is the first demonstration of a link between behavioral performance and the timescale of metastable dynamics in PFdl neurons during a decision.

Comparison with previous studies on error-related activity in prefrontal cortex

The results reported here were obtained via an HMM analysis of ensemble activity. HMM analysis and its variations (Blaettler et al., 2011; Chen, 2013) present an ideal method to investigate the role of metastable dynamics. HMM allows an unsupervised segmentation of the ensemble activity without relying on external triggers, providing a characterization of the metastable dynamics during ongoing activity or motor preparation, not just after a stimulus (Abeles et al., 1995; Seidemann et al., 1996; Mazzucato et al., 2015). In particular, this allows one to pinpoint the moment in time in which an internal deliberation may have occurred. This is essential in trying to link behavior to neural activity occurring during internal deliberation as done here, and this has allowed us to find neural correlates of trial difficulty and behavioral performance that had not emerged from single-neuron analyses (Genovesio et al., 2011).

We note that our approach is very different from those of previous HMM studies of error activity, wherein an HMM fitted to trials in a given condition (say, S1>S2) was used to predict errors in a separate condition (S2<S1) (Ponce-Alvarez et al., 2012; Seidemann et al., 1996; Jones et al., 2007). In contrast, our ability to predict errors is based on the modulation of the dynamics of the same HMM. Our analysis on mean state durations uncovered a change in the network dynamics during incorrect trials that manifests itself as a reduced transition rate among successive states. Thus, errors are not predicted by the presence of

specific “error states” but rather by the slowing down of state sequences that may be the same in either condition.

Our approach is also different from previous studies that have examined PFdl activity during errors based on the activity of single neurons. From these studies, the picture has emerged that PFdl neurons encode the adopted course of action during errors rather than the correct course of action. PFdl activity reflected the target chosen during errors in a motion discrimination task (Kim and Shadlen, 1999) and in a match-to-sample task for visual motion (Zaksas and Pasternak, 2006). Similar results were observed in tasks that required learning of action sequences, wherein PFdl neuronal activity reflected either the incorrect oculomotor sequence of actions (Averbeck and Lee, 2007) or the incorrect category of turn, pull, and push hand movements during errors (Shima et al., 2007). At a more abstract level, PFdl neurons appear to encode goal and strategy in a task in which the goal was chosen after the selection of either a repeat-stay or a change-shift strategy (Genovesio et al., 2008). These strategies required selection of the same or a different goal when a central instruction stimulus repeated or changed from the previous trial, respectively. PFdl neurons encoding the future goal appeared to encode the chosen goal rather than the correct goal during the decision period; however, strategy-coding neurons reflected the strategy adopted (rather than the correct strategy) only after the action. In Tsujimoto et al. (2011), a simplified version of the strategy task was adopted in which the shape and color of a cue stimulus indicated which strategy to use. This task required a more immediate strategy selection that was not based on the integration of previous events as in Genovesio et al. (2005, 2008). In this case, during the decision period, PFdl neurons encoded the strategy selected and not the strategy that had been cued. Interestingly, orbitofrontal neurons in the same task had the opposite behavior.

Finally, previous studies have shown the effect of previous trials on the activity of single neurons in the current trial. For example, Donahue et al. (2013) had shown the impact of reward on encoding of previous choice in multiple cortical areas, while a recent study by Spitmaan et al. (2020) has shown that both reward and choice outcomes are integrated over multiple trials to influence behavior and the response of cortical neurons. In the task studied here, we had found (Genovesio et al., 2014) that past outcome affected the RTs but not the error rates, and only a very small effect of the previous choice on RTs. These results suggest that, in our task, past outcome could have an influence on the metastable activity of PFdl neurons in the present trial. This influence could be revealed by the presence of coding states for the previous outcome. However, although single neurons encode both the previous choice and the previous outcome in the earlier part of the present trial before S2 (Genovesio et al., 2014), we found no evidence of coding states for previous outcome or choice during the temporal window analyzed in this paper (400 ms before S2 until the end of the trial; data not shown). This suggests that the slowdown of dynamics between S2 and the GO signal reflects the task demands of the present trial in a larger measure rather than the properties of the previous trial, although it cannot be ruled out that history effects could emerge in an HMM analysis performed in an earlier portion of the trial or in datasets containing larger numbers of neurons.

Link between single neurons and metastable ensemble activity

The studies reviewed earlier focused on the activity of single neurons taken individually rather than on ensemble dynamics, as done here. It is natural to assume a link between the activity of single neurons and the sequence of states of the ensemble activity. We propose here one possibility based on our previous work on the evolution of goal representation in this task (Marcos et al., 2019). After the GO signal, we observed an abrupt reconfiguration of the prefrontal activity, in which the goal signal passed from one population to another as the trial proceeded from the delay period to the action period; only a smaller subset of neurons coded goals across both periods, and about half of these neurons switched goal preference between trial periods ("switch neurons"). These results were modeled by a network of heterogeneous cell assemblies with bistable local dynamics. In the model, the switch neurons showed a higher level of bursting activity than the other neurons, indicating that these neurons tended to jump more easily from high to low firing states, and vice versa. The switch neurons appeared also to have a leading role in the network reconfiguration after the GO signal, showing an earlier transition time in activity switch. It is possible that, when analyzed in terms of switching ensemble states via an HMM, the switch neurons could play an important role in igniting state transitions and could act differently in correct versus error trials. The important connection between single-cell and ensemble dynamics is left for future studies.

STAR★METHODS

RESOURCE AVAILABILITY

Lead contact—Further information should be directed to and will be fulfilled by the Lead Contact, Aldo Genovesio (aldo.genovesio@uniroma1.it)

Materials availability—This study did not generate new unique reagents.

Data and code availability—The in-house code developed during this study is publicly available in the author's GitHub repository at https://github.com/danilobenozzo/hmm_neurofis. The dataset has not been deposited in a public repository but is available from the Lead Contact author upon request.

EXPERIMENTAL MODEL AND SUBJECT DETAILS

In this study we used two adult (aged 9 and 11 years old), male rhesus monkeys (Macaca mulatta). Monkey 1 weighed 8.5 kg, and monkey 2 weighed 8.0 kg. All procedures followed the National Institutes of Health Guide for the Care and Use of Laboratory Animals (1996) and were approved by the National Institute of Mental Health Animal Care and Use Committee.

METHOD DETAILS

Behavioral task—In each trial, two visual stimuli were presented in sequence on a computer screen, separated by a temporal delay (Figure 1A). Each stimulus could be either a blue circle of 3° diameter or a red square of 3×3° dimension. If the first stimulus (S1) was the red square then the second stimulus (S2) was the blue circle and vice versa. Each

stimulus remained on screen for 1000 ms. Each trial started when the monkeys pressed the central of three switches, which caused the appearance on the screen of a central stimulus (reference point). After 400 or 800 ms the central stimulus was followed by the onset of S1. S1 was always located at a distance of 8–48 mm (in steps of 8 mm) above or below the reference point. After the disappearance of S1, there was a first delay (D1) of 400 or 800 ms before the presentation of S2. S2 appeared above the reference point if S1 had appeared below, and below the reference point otherwise. Its distance was as for S1, i.e., 8–48 mm (in steps of 8 mm) above or below the reference point, but it never equaled the distance of S1. Both S1 and S2 were presented for 1000 ms. The disappearance of S2 was followed by a second delay (D2) of 0, 400 or 800 ms, which in turn preceded the reappearance of the two stimuli, which served as a “GO” signal. Each stimulus was pseudo-randomly chosen to be located either 40 mm to the right or 40 mm to the left of the central stimulus. The monkeys were required to select, within 6 s, the stimulus presented farther from the reference point. Note that, not knowing the location of the stimuli, the monkeys could not plan any motor response before the GO signal. Correct choices were rewarded with 0.1 mL fluid, whereas an acoustic feedback followed the errors. All task variables, such as the duration of D1 and D2, the color and the shape of the two stimuli, were pseudorandomly determined. For more details about the behavioral task see Genovesio et al. (2011).

Data collection—We monitored and recorded eye position with an infrared oculometer (Arrington Recording, Scottsdale, AZ, USA) and recorded single cells using quartz insulated, platinum-iridium electrodes (0.5–1.5 MΩ at 1 kHz), positioned by a 16-electrode drive assembly (Thomas Recording, Giessen, Germany). The electrodes were arranged within a concentric head with 518 mm spacing. Spikes were discriminated online using the Multichannel Acquisition Processor (Plexon, Dallas, TX, USA) and confirmed with the Offline Sorter (Plexon) based on principal component analysis, minimal interspike intervals, and well differentiated waveforms inspected individually for each isolated neuron.

Surgery—We implanted the recording chambers over the exposed dura mater of the left frontal lobe, along with head restraint devices. We used Aseptic techniques together with isofluorane anesthesia (1%–3%, to effect). Monkey 1 had two, 18 mm diameter chambers, and Monkey 2 had a single, 27×36 mm chamber.

Histological analysis—Before the end of the recordings, electrolytic lesions (15 mA for 10 s, anodal current) were made at selected locations. After 10 days, the animal was deeply anesthetized and then perfused through the heart with formaldehyde-containing fixative (10% Formalin in 0.9% saline). We plotted recording sites on Nissl-stained coronal sections by reference to the recovered electrolytic lesions and the marking pins inserted during perfusion, and structural magnetic resonance images taken at various stages after the beginning of the recordings. Recordings were predominantly taken from area 8, area 46 and a small population of area 12.

HMM analysis—An HMM was used to study the dynamics of neural ensembles, with methodology similar to Ponce-Alvarez et al., (2012) and Mazzucato et al. (2015, 2016, 2019). The sessions included in the analysis comprised at least 4 simultaneously recorded

neurons, each with a mean trial activity ≥ 1 spk/s, and with at least 5 completed trials of each type, i.e., correct and incorrect. These selection rules left about 20% of the sessions for further analysis, out of the 361 initially recorded. Since many PFC neurons code for stimulus position (Genovesio et al., 2011), trials of the same session were divided according to the up or down position of the second stimulus, and were analyzed by fitting separate HMMs (in the analysis of trial difficulty of Figure 6, similar results were obtained when fitting the same HMM to all correct trials in each session, see "Analysis of neural dynamics versus trial difficulty"). In addition, in the analysis of correct versus error trials (Figures 2, 3, 4, and 5), HMMs were also fitted separately to correct versus error trials in each session (see "Analysis of neural dynamics in correct versus error trials" below). In all HMM analyses described below, the vector of the neurons' average firing rates across trials was used to initialize the emission rates for the first state. The same vector was then randomly permuted and assigned to the next state, until all states' emission rates were initialized. In addition to a random permutation, a random Gaussian component with zero mean and 0.02 std was added to each emission rate. The transition matrix P_{ij}, expressing the transition rates from state i to state j in each 5 ms bin, was initialized to 1 for the diagonal entries and $|0.02x|$ off the diagonal, where x is a standard random variable; the rows of the matrix were then normalized to obtain probabilities. This initialization corresponds to a model where the probability is much larger to remain in the current state than to make a transition to another state in the next time bin. The fitting procedure was repeated 5 times with a maximum number of 500 iterations. The model with the smallest Bayesian Information Criterion (BIC) score, $\mathrm{BIC} = -2\,\mathrm{LL} + [M(M-1) + MN]\ln T$, was selected as the model for further analysis, where LL is the log-likelihood of the model given the data, M is the number of hidden states, N is the number of neurons in the ensemble, and T is the number of observations in each session (number of trials × number of 5 ms bins per trial). A cross-validation procedure as performed e.g., in Maboudi et al. (2018) gave similar results (not shown).

The training phase of the model, consisting in the estimation of the transition and emission probability matrices, was performed using the Baum-Welch algorithm. The states were then decoded from the posterior state probabilities $P(S_t|X_t)$ of having state S_t in the presence of data X_t (spike trains) in a 5 ms time bin centered around time t. We assigned a state to a chunk of data only if its posterior probability was greater than 0.8 for at least 50 consecutive ms, as this requirement reduces the chance of overfitting the data (Mazzucato et al., 2015, 2016).

All analyses were performed using custom software written in Python and MATLAB (Statistics and Machine Learning Toolbox, ©The Mathworks). The code is available at https://github.com/danilobenozzo/hmm_neurofis.

Coding states—The presence of a coding state, meaning a state that codes for a specific task condition, was evaluated by a χ-squared test of the frequency of appearance of each state in a given task condition during a time window of interest. The frequency table was computed by reporting the frequency of occurrence of each state in the two task conditions to be compared. As task condition, we considered the relative distance of the two stimuli from the center based on stimulus features (blue circle versus red square) and order of presentation (S2 farther versus closer), and position of the target at GO (right versus left; the

target is the stimulus previously presented farther from the center). As for the time window of interest, we chose the S2 presentation period for states coding for relative distance based on stimulus features or order, and the time interval from GO to RT for the target position.

Shuffled datasets—The HMM analysis was validated via comparison with shuffled data. Three types of shuffling procedures were applied in each session: a circular shuffle, a swap shuffle, and class label shuffle. In the latter, the class labels associated with each trial type (S1> S2 versus S2>S1) were randomly shuffled. Circular shuffle (Maboudi et al., 2018) consisted of independent random time shifts of the spike trains in each trial. This procedure kept the single neuron autocorrelations intact but disrupted the cross-correlations across neurons and, in particular, instances of co-activation. Swap shuffles (Maboudi et al., 2018) randomly permuted the temporal bins, i.e., the vectors of spike counts, in each trial. This procedure preserved the neurons' cross-correlations but removed the neurons' autocorrelations, in addition to the order of the sequential patterns that might be present in the data. Note that neither procedure changed the overall firing rates of the neurons in each trial. The HMM fits of the shuffled datasets were compared with the fit of the original dataset in terms of BIC score and optimal number of states. For the sake of visualization, in Figures 3A–3C time has been uniformly warped in the main task epochs (e.g., S2 presentation, delay D2, reaction time) by a normalization with respect to each epoch length in order to align the related events across trials.

Analysis of neural dynamics in correct versus error trials—To compare state durations in correct and error trials, the HMM was fitted to all data inside a time window of variable size starting 400 ms before S2 and ending at the beginning of the following trial. Trials of the same session were divided according to the up or down position of the second stimulus and into correct versus error, and were analyzed by fitting four separate HMMs in each condition (56 sessions in total). In each session, we used models with 2 to $N-1$ states, where N is the number of neurons in the session (the number of states was kept lower than the number of neurons to help prevent overfitting). The optimal number of states in each session, M, was chosen so as to minimize the BIC score (see formula reported above). Two separate HMMs were fitted to correct and incorrect trials in the same session given the stimulus position. After decoding the data according to the posterior state probabilities $P(S_t|X_t)$ as described above, we compared the session-averaged state durations in correct versus error trials in two different time epochs, from offset of S2 to GO, and from GO to END, by performing a 2-way ANOVA with factors trial type (correct versus error) and time epoch. To validate the analysis with a balanced number of trials in each trial type (correct versus error), we randomly selected a number of correct trials matching the number of error trials in each session. The HMM analysis was performed on the trial-matched sessions as described above, and the mean state durations in correct versus error trials across all sessions were obtained. This procedure was repeated 20 times, each time with a new pseudo-random selection of correct trials. These same trial-balanced datasets were then analyzed after circularly shuffling each spike train (see Section "Shuffled datasets"). Swap-shuffling the data drastically reduced the number of states and transitions and resulted in only a handful of trials with at least 2 transitions in each session, precluding a meaningful analysis of the state durations in this case.

ROC analysis—We used the distributions of mean state durations from S2 to GO obtained as described in Section "Analysis of neural dynamics in correct versus error trials" to predict the performance (correct versus error) in single trials. To do so, we treated the task of predicting performance as a fictitious two-alternative forced choice (2AFC) task in which we are presented with a correct and an error trial, and for each such pair, we predict that the error trial is the one with longer mean state duration. Performance in this task can be obtained by computing the area under the receiver operating characteristic (ROC) curve (Dayan and Abbott, 2005). The latter is the curve plotting the fraction of true positives (hits) versus the fraction of false positives (false alarms) obtained as the decision threshold varies from $+\infty$ to $-\infty$, where the task is to classify single trials and each decision is based on whether the trial's mean state duration is above or below the threshold. Note that this analysis is analogous to that performed in Britten et al. (1992) for decoding motion direction from single neurons' firing rates. However, in Britten et al. (1992) the authors aimed to decode the stimulus while we aimed to decode the monkeys' performance (correct versus error). In the latter case, the prediction of a correct trial corresponds to matching the monkeys' behavior in that trial. Thus, our average decoding performance also gives the probability of predicting the monkey's behavior on a trial-by-trial basis.

Analysis of neural dynamics versus trial difficulty—For this analysis, we fitted an HMM to the data inside a 1400 ms time window (400 ms before the presentation of S2 until its removal), and the number of states was set to 2 (Ponce-Alvarez et al., 2012). Only correct trials were used, divided according to the up or down position of the second stimulus, and then analyzed by fitting separate HMMs (however, similar results were obtained when fitting the same HMM to all correct trials in each session; not shown). We defined the time until the first transition after S2 (fTaS2) as the period of time between S2 onset and the time at which the posterior probability of the current state decreases below 0.8 (see Figure 6 for examples). fTaS2 times were regressed with |S2–S1| as described in Results. In this analysis, only sessions with significant decoding performance by the HMM were considered (41 out of 61 sessions with S2 up and 34/61 sessions with S2 down), according to the following procedure (Ponce-Alvarez et al., 2012). We divided each session in testing and training sets in a 3-fold cross-validation framework. For each trial in the testing set, its log-likelihood was computed both by a model fitted in the training trials of class S1>S2 (model λ_1) and by a model fitted in the training trials of class S2>S1 (model λ_2; here, "S1>S2" means that S1 was more distant than S2 from the central stimulus). The tested trial was assigned to class S1>S2 if model λ_1 had the larger log-likelihood on this trial, and to class S2>S1 otherwise. The session was kept for further analysis if the decoding performance of the above method, measured by balanced accuracy, was significantly larger than chance. Balanced accuracy was defined as the average of recall obtained on each class, i.e., 1=2(TP/P+TN/N), and was used because in most sessions the two classes S1>S2 and S2>S1 were unbalanced (i.e., there were an unequal number of trials in each class; see Brodersen et al., 2010 for details). Here, TP means "true positives," TN means "true negatives," and P, N stands for positive (i.e., elements of class S1>S2) and negative (elements of class S2> S1), respectively. Significance of the decoder's balanced accuracy was computed by a binomial test at the 5% significance level. The same analysis was performed after shuffling the data as described in Section "Shuffled datasets."

QUANTIFICATION AND STATISTICAL ANALYSIS

- HMM analysis: discrete time HMM with Poisson emission probability, model estimation solved by the iterative Baum-Welch algorithm as implemented in the MATLAB functions *hmmtrain* and *hmmdecode*, and with BIC method to select the optimal number of states (see Figure 2);
- Shuffling procedure to validate the HMM results: circular and swap shuffling (see Shuffled datasets in Section STAR Methods for details and Figure 3);
- Coding state: χ-squared test applied on the frequency of appearance of each state in a given task condition during a time window of interest (see Figure 4);
- Analysis between correct and error trials: two-sided Mann-Whitney U test, Spearman's rank correlation, Wilcoxon signed-rank test and two-way ANOVA (see Figure 5);
- Relation with trial difficulty: Jonckheere's trend test and linear regression slope (see Figure 6).

Further statistical details are indicated in each figure legend and in Section Results.

ACKNOWLEDGMENTS

We thank Dr. Steven P. Wise, Dr. Satoshi Tsujimoto, and Andrew Mitz for their contributions in the experimental phase of the study. This work has been partially supported by a grant from Sapienza University of Rome (Progetto H2020: PH1181642DB714F6) to A.G. and by an NIH/NINDS Brain Initiative grant (1UF1NS115779) and a grant from the Office of the Vice President for Research of Stony Brook University (award 1153707-2-63845) to G.L.C. The data analyzed in this article were collected at the National Institute of Mental Health, with support from the Division of Intramural Research. The views expressed in this article do not necessarily represent the views of the NIMH, NIH, or the U.S. Government.

REFERENCES

Abeles M, Bergman H, Gat I, Meilijson I, Seidemann E, Tishby N, and Vaadia E (1995). Cortical activity flips among quasi-stationary states. Proc. Natl. Acad. Sci. USA 92, 8616–8620. [PubMed: 7567985]

Averbeck BB, and Lee D (2007). Prefrontal neural correlates of memory for sequences. J. Neurosci. 27, 2204–2211. [PubMed: 17329417]

Bewick V, Cheek L, and Ball J (2004). Statistics review 10: further nonparametric methods. Crit. Care 8, 196–199. [PubMed: 15153238]

Blaettler F, Kollmorgen S, Herbst J, and Hahnloser R (2011). Hidden Markov models in the neurosciences. In Hidden Markov Models: Theory and Applications, Dymarski P, ed. (IntechOpen), pp. 169–186.

Britten KH, Shadlen MN, Newsome WT, and Movshon JA (1992). The analysis of visual motion: a comparison of neuronal and psychophysical performance. J. Neurosci. 12, 4745–4765. [PubMed: 1464765]

Brodersen KH, Ong CS, Stephan KE, and Buhmann JM (2010). The Balanced Accuracy and Its Posterior Distribution. In 20th International Conference on Pattern Recognition, A. Erçil, General Chair (IEEE: Institute of Electrical and Electronics Engineers), pp. 3121–3124.

Chen Z (2013). An overview of Bayesian methods for neural spike train analysis. Comput. Intell. Neurosci. 2013, 251905. [PubMed: 24348527]

Dayan P, and Abbott LF (2005). Theoretical Neuroscience: Computational and Mathematical Modeling of Neural Systems (MIT Press).

Donahue CH, Seo H, and Lee D (2013). Cortical signals for rewarded actions and strategic exploration. Neuron 80, 223–234. [PubMed: 24012280]

Engel TA, Steinmetz NA, Gieselmann MA, Thiele A, Moore T, and Boahen K (2016). Selective modulation of cortical state during spatial attention. Science 354, 1140–1144. [PubMed: 27934763]

Freedman DJ, Riesenhuber M, Poggio T, and Miller EK (2001). Categorical representation of visual stimuli in the primate prefrontal cortex. Science 291, 312–316. [PubMed: 11209083]

Genovesio A, Brasted PJ, Mitz AR, and Wise SP (2005). Prefrontal cortex activity related to abstract response strategies. Neuron 47, 307–320. [PubMed: 16039571]

Genovesio A, Tsujimoto S, and Wise SP (2008). Encoding problem-solving strategies in prefrontal cortex: activity during strategic errors. Eur. J. Neurosci. 27, 984–990. [PubMed: 18279367]

Genovesio A, Tsujimoto S, and Wise SP (2009). Feature- and order-based timing representations in the frontal cortex. Neuron 63, 254–266. [PubMed: 19640483]

Genovesio A, Tsujimoto S, and Wise SP (2011). Prefrontal cortex activity during the discrimination of relative distance. J. Neurosci. 31, 3968–3980. [PubMed: 21411640]

Genovesio A, Tsujimoto S, and Wise SP (2012). Encoding goals but not abstract magnitude in the primate prefrontal cortex. Neuron 74, 656–662. [PubMed: 22632724]

Genovesio A, Tsujimoto S, Navarra G, Falcone R, and Wise SP (2014). Autonomous encoding of irrelevant goals and outcomes by prefrontal cortex neurons. J. Neurosci. 34, 1970–1978. [PubMed: 24478376]

Hoshi E, Shima K, and Tanji J (2000). Neuronal activity in the primate prefrontal cortex in the process of motor selection based on two behavioral rules. J. Neurophysiol. 83, 2355–2373. [PubMed: 10758139]

Jones LM, Fontanini A, Sadacca BF, Miller P, and Katz DB (2007). Natural stimuli evoke dynamic sequences of states in sensory cortical ensembles. Proc. Natl. Acad. Sci. USA 104, 18772–18777. [PubMed: 18000059]

Kemere C, Santhanam G, Yu BM, Afshar A, Ryu SI, Meng TH, and Shenoy KV (2008). Detecting neural-state transitions using hidden Markov models for motor cortical prostheses. J. Neurophysiol. 100, 2441–2452. [PubMed: 18614757]

Kim JN, and Shadlen MN (1999). Neural correlates of a decision in the dorsolateral prefrontal cortex of the macaque. Nat. Neurosci. 2, 176–185. [PubMed: 10195203]

La Camera G, Fontanini A, and Mazzucato L (2019). Cortical computations via metastable activity. Curr. Opin. Neurobiol. 58, 37–45. [PubMed: 31326722]

Linderman SW, Johnson MJ, Wilson MA, and Chen Z (2016). A Bayesian nonparametric approach for uncovering rat hippocampal population codes during spatial navigation. J. Neurosci. Methods 263, 36–47. [PubMed: 26854398]

Maboudi K, Ackermann E, de Jong LW, Pfeiffer BE, Foster D, Diba K, and Kemere C (2018). Uncovering temporal structure in hippocampal output patterns. eLife 7, e34467. [PubMed: 29869611]

Maoz U, Rutishauser U, Kim S, Cai X, Lee D, and Koch C (2013). Pre-deliberation activity in prefrontal cortex and striatum and the prediction of subsequent value judgment. Front. Neurosci. 7, 225. [PubMed: 24324396]

Marcos E, and Genovesio A (2016). Determining Monkey Free Choice Long before the Choice Is Made: The Principal Role of Prefrontal Neurons Involved in Both Decision and Motor Processes. Front. Neural Circuits 10, 75. [PubMed: 27713692]

Marcos E, Tsujimoto S, and Genovesio A (2017). Independent coding of absolute duration and distance magnitudes in the prefrontal cortex. J. Neurophysiol. 117, 195–203. [PubMed: 27760814]

Marcos E, Tsujimoto S, Mattia M, and Genovesio A (2019). A Network Activity Reconfiguration Underlies the Transition from Goal to Action. Cell Rep. 27, 2909–2920.e4. [PubMed: 31167137]

Mazzucato L, Fontanini A, and La Camera G (2015). Dynamics of multistable states during ongoing and evoked cortical activity. J. Neurosci. 35, 8214–8231. [PubMed: 26019337]

Mazzucato L, Fontanini A, and La Camera G (2016). Stimuli reduce the dimensionality of cortical activity. Front. Syst. Neurosci. 10, 11. [PubMed: 26924968]

Mazzucato L, La Camera G, and Fontanini A (2019). Expectation-induced modulation of metastable activity underlies faster coding of sensory stimuli. Nat. Neurosci. 22, 787–796. [PubMed: 30936557]

Miller P, and Katz DB (2010). Stochastic transitions between neural states in taste processing and decision-making. J. Neurosci. 30, 2559–2570. [PubMed: 20164341]

Moran A, and Katz DB (2014). Sensory cortical population dynamics uniquely track behavior across learning and extinction. J. Neurosci. 34, 1248–1257. [PubMed: 24453316]

Pardo-Vazquez JL, Leboran V, and Acuña C (2008). Neural correlates of decisions and their outcomes in the ventral premotor cortex. J. Neurosci. 28, 12396–12408. [PubMed: 19020032]

Ponce Alvarez A, Kilavik B, and Riehle A (2008). Dynamic sequences of states in ensembles of motor cortical neurons. In Deuxième Conférence Française de Neurosciences Computationnelles, “Neurocomp08” [Proceedings of the Second French Conference on Computational Neuroscience, ”Neurocomp08”, Marseille. LU France Perrinet., and Daucé E, eds., pp. 251–254.

Ponce-Alvarez A, Nácher V, Luna R, Riehle A, and Romo R (2012). Dynamics of cortical neuronal ensembles transit from decision making to storage for later report. J. Neurosci. 32, 11956–11969. [PubMed: 22933781]

Recanatesi S, Pereira U, Murakami M, Mainen Z, and Mazzucato L (2020). Metastable attractors explain the variable timing of stable behavioral action sequences. bioRxiv. 10.1101/2020.01.24.919217.

Rich EL, and Wallis JD (2016). Decoding subjective decisions from orbitofrontal cortex. Nat. Neurosci. 19, 973–980. [PubMed: 27273768]

Rich EL, Stoll FM, and Rudebeck PH (2018). Linking dynamic patterns of neural activity in orbitofrontal cortex with decision making. Curr. Opin. Neurobiol. 49, 24–32. [PubMed: 29169086]

Sadacca BF, Mukherjee N, Vladusich T, Li JX, Katz DB, and Miller P (2016). The behavioral relevance of cortical neural ensemble responses emerges suddenly. J. Neurosci. 36, 655–669. [PubMed: 26791199]

Seidemann E, Meilijson I, Abeles M, Bergman H, and Vaadia E (1996). Simultaneously recorded single units in the frontal cortex go through sequences of discrete and stable states in monkeys performing a delayed localization task. J. Neurosci. 16, 752–768. [PubMed: 8551358]

Shima K, Isoda M, Mushiake H, and Tanji J (2007). Categorization of behavioural sequences in the prefrontal cortex. Nature 445, 315–318. [PubMed: 17183266]

Spitmaan M, Seo H, Lee D, and Soltani A (2020). Multiple timescales of neural dynamics and integration of task-relevant signals across cortex. Proc. Natl. Acad. Sci. USA 117, 22522–22531. [PubMed: 32839338]

Taghia J, Cai W, Ryali S, Kochalka J, Nicholas J, Chen T, and Menon V (2018). Uncovering hidden brain state dynamics that regulate performance and decision-making during cognition. Nat. Commun. 9, 2505. [PubMed: 29950686]

Tanji J, and Hoshi E (2001). Behavioral planning in the prefrontal cortex. Curr. Opin. Neurobiol. 11, 164–170. [PubMed: 11301235]

Tsujimoto S, Genovesio A, and Wise SP (2011). Comparison of strategy signals in the dorsolateral and orbital prefrontal cortex. J. Neurosci. 31, 4583–4592. [PubMed: 21430158]

Zaksas D, and Pasternak T (2006). Directional signals in the prefrontal cortex and in area MT during a working memory for visual motion task. J. Neurosci. 26, 11726–11742. [PubMed: 17093094]

Highlights

- Prefrontal activity in monkeys performing a distance discrimination task is metastable
- Duration of metastable states is longer before errors
- Latency of state transition is longer in correct difficult trials
- States may code for relative distance based on stimulus features or presentation order

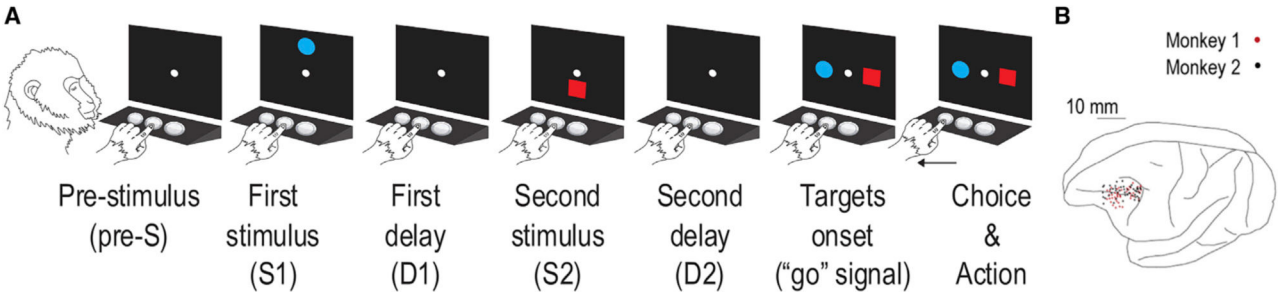

Figure 1. Experimental paradigm and neural recordings sites

(A) Sequence of task events within a trial. Each trial started when the monkey touched the central switch, leading to the appearance of the central stimulus (reference point), which lasted for 400 or 800 ms (pre-stimulus; pre-S). After this pre-stimulus period, the first stimulus (S1) was presented. S1 was followed by a variable delay (first delay; D1) of 400 or 800 ms, which lasted until the second stimulus (S2) appeared. S2 was followed by a second delay (D2) of 0, 400, or 800 ms. Both S1 and S2 were presented for 1,000 ms and placed either above or below the reference point at 8 to 48 mm (8-mm step) from the reference point. After both stimuli reappeared (placed horizontally), the monkey had to touch the switch below the stimulus that appeared farther from the reference point (the blue circle in the example trial). Correct responses were rewarded with 0.1 mL fluid, while errors were followed by an acoustic feedback. The stimulus feature (blue circle/red square), position (above/below the reference point), distance, and target position (left/right) were pseudo-randomly selected.

(B) Penetration sites. Composite from both monkeys, relative to sulcal landmarks. See STAR Methods for details.

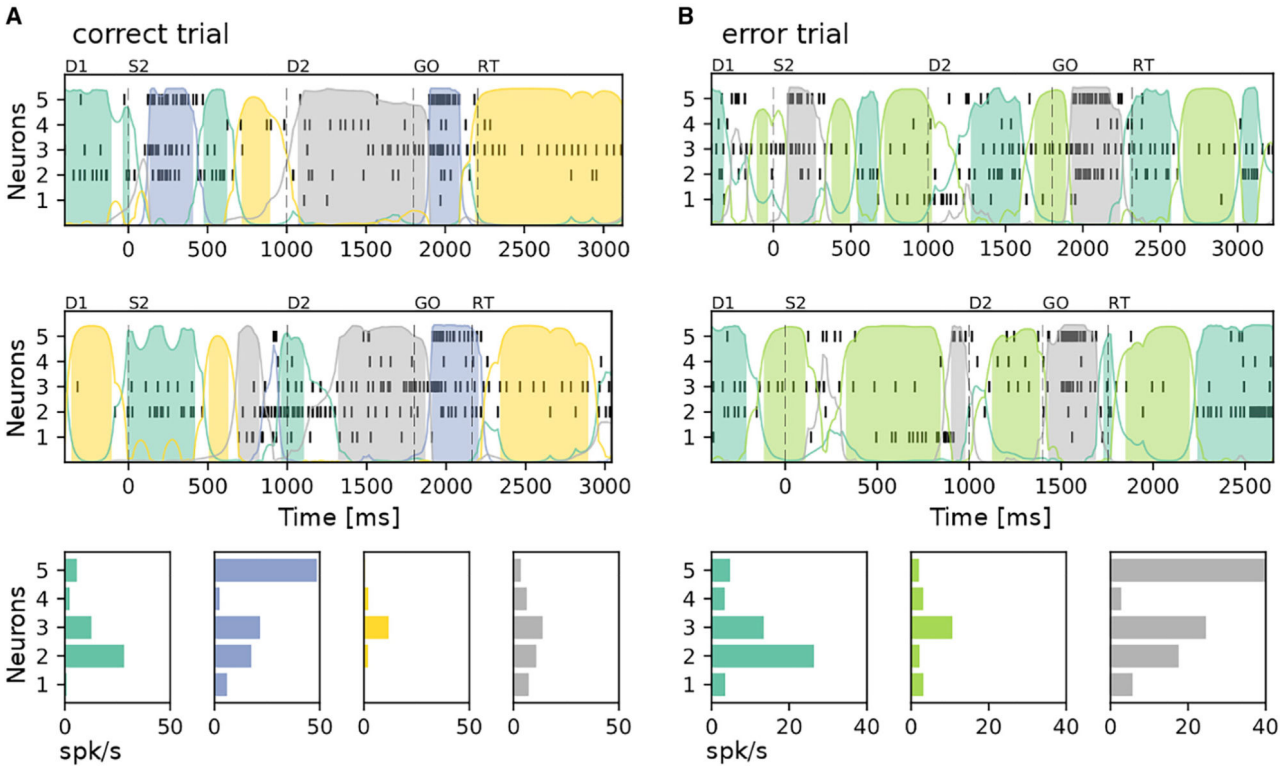

Figure 2. Representative trials of a neural ensemble of simultaneously recorded cells

Each raster plot indicates the spiking activity of each recorded neuron from 400 ms before S2 presentation until the beginning of the following trial. Colored curves represent the posterior state probabilities, and the assigned states are indicated with colored areas. Insets (bottom panels) indicate firing rate vectors associated with each state (same color code as in corresponding top panels). (A) Correct trials. (B) Error trials. Note that similar colors in (A) and (B) do not correspond to similar states, since the HMMs were performed independently on correct and error trials (see STAR Methods). D1, first delay (after S1); S2, second stimulus; D2, second delay; GO, appearance of targets on screen; RT, reaction time.

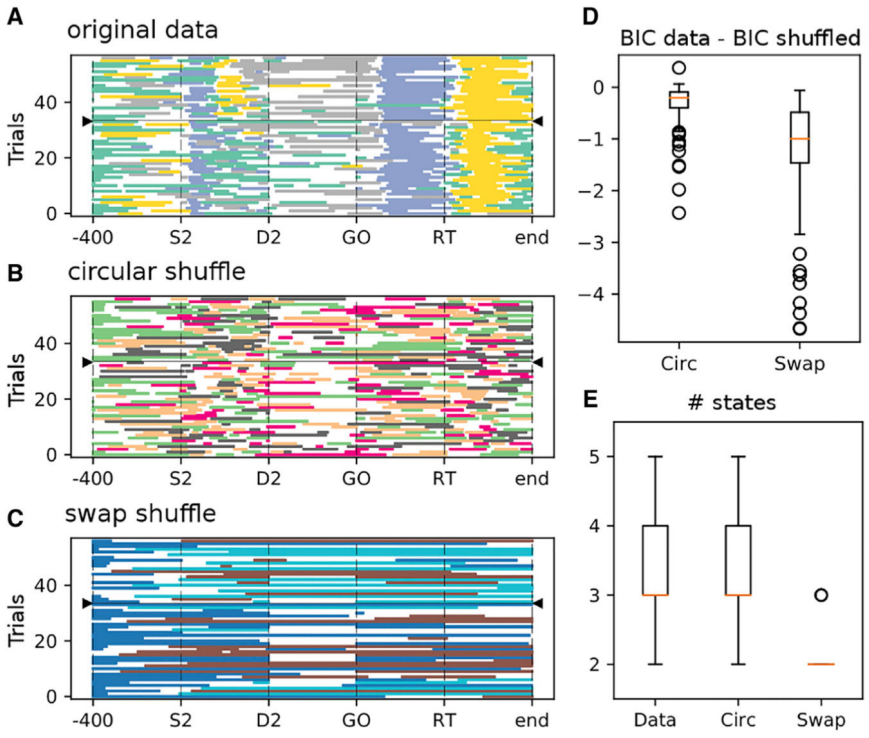

Figure 3. Comparison of HMM state sequences for original and shuffled datasets

(A–C) Comparison of HMM state sequences for original and shuffled datasets in one representative session (only trials with S2 in the UP position are indicated; similar plots are obtained in other conditions). Trials were grouped according to the relative distance based on stimulus features (blue circle versus red square), and the separation between the two groups is indicated by the black horizontal line with borders marked by triangles (with red trials above the line). The time in each trial has been warped (stretched or shrunk; see STAR Methods) so as to align the 4 events S2, D2, GO, and RT. (A) HMM model of original data reveals (1) the presence of a coding state for relative distance based on stimulus features (the yellow state appearing between S2 and D2 only in trials above the group separation line, coding for “red square farther”) and (2) reliable state transitions at relevant event times. (B) HMM model of circularly shuffled data indicated in (A). As a consequence, state sequences appear scrambled, and the coding states are lost. (C) HMM model of swap-shuffled data indicated in (A). Compared to (A), sequences are not orderly, despite the presence of fewer states. (D) Boxplots of the difference in BIC score between the fits to the original data and shuffled data across sessions ($p < 0.001$, Wilcoxon signed-rank test). A smaller score indicates better fit.

(E) Optimal number of inferred states across sessions for original data (left), circular-shuffled data (middle), and swap-shuffled data (right). Note that similar color in panels a-c does not imply the same state.

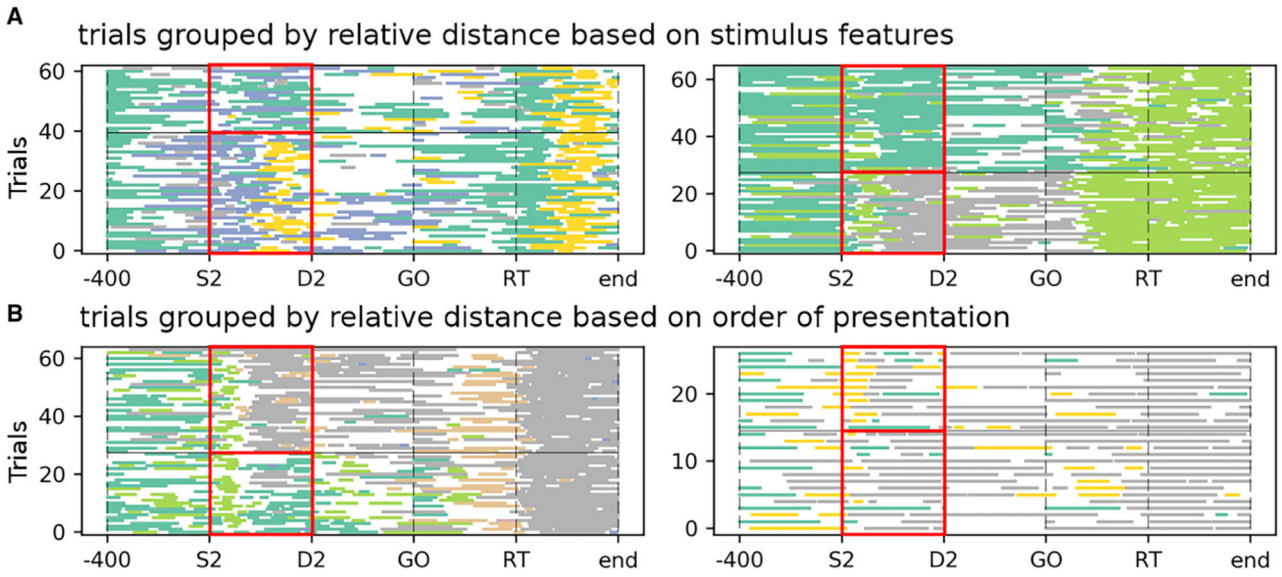

Figure 4. Examples of sessions with significant coding states

(A) Coding states for relative distance based on stimulus features (blue circle versus red square) during S2 (red box) in correct trials for 2 example sessions. Coding states are the dark green and yellow states in the left panel and the dark green and gray states in the right panel.

(B) Coding states for relative distance based on order of presentation during S2 (S2 farther versus S2 closer) in correct trials for 2 example sessions. Coding states are the dark green, orange, and gray states in the left panel and the yellow state in the right panel. In both panels, trials were grouped according to the coded variable (as in Figure 3A) and highlighted by the red box. The same colors in different panels do not imply the same state.

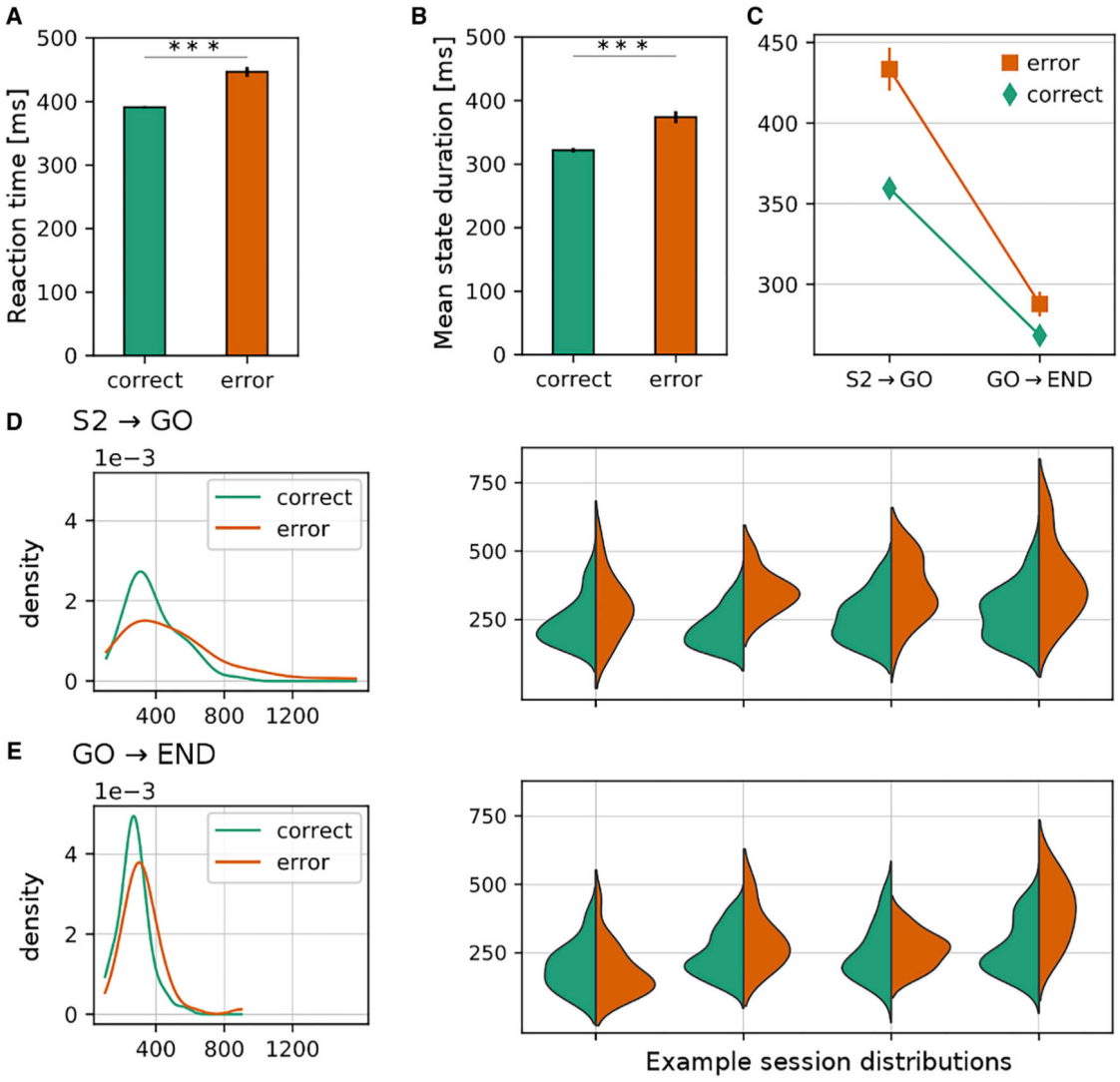

Figure 5. Comparison of RTs and mean state durations between correct and incorrect trials

The mean values ± SEM are reported. ***p < 0.001, two-sided Mann-Whitney U test. Correct trials are indicated in green; incorrect trials are indicated in red.

(A) Reaction times (RTs).

(B) Mean state durations.

(C) Comparison of mean state durations in the S2-GO versus the GO-END intervals, divided into correct and error trials. The plot indicates the interaction plot of the two-way ANOVA, with factors Trial Type ($p < 10^{-12}$, $F(1) = 50.9$) and Temporal Window ($p = 0$, $F(1) = 363.6$ p(interaction) $< 10^{-5}$, $F(1) = 16.3$).

(D) Left: distributions of mean state durations across sessions in the S2-GO period in correct and error trials. Right: distributions of state durations in 4 example sessions (green, correct trials; red, error trials).

(E) Same as in (D) for the GO-END period.

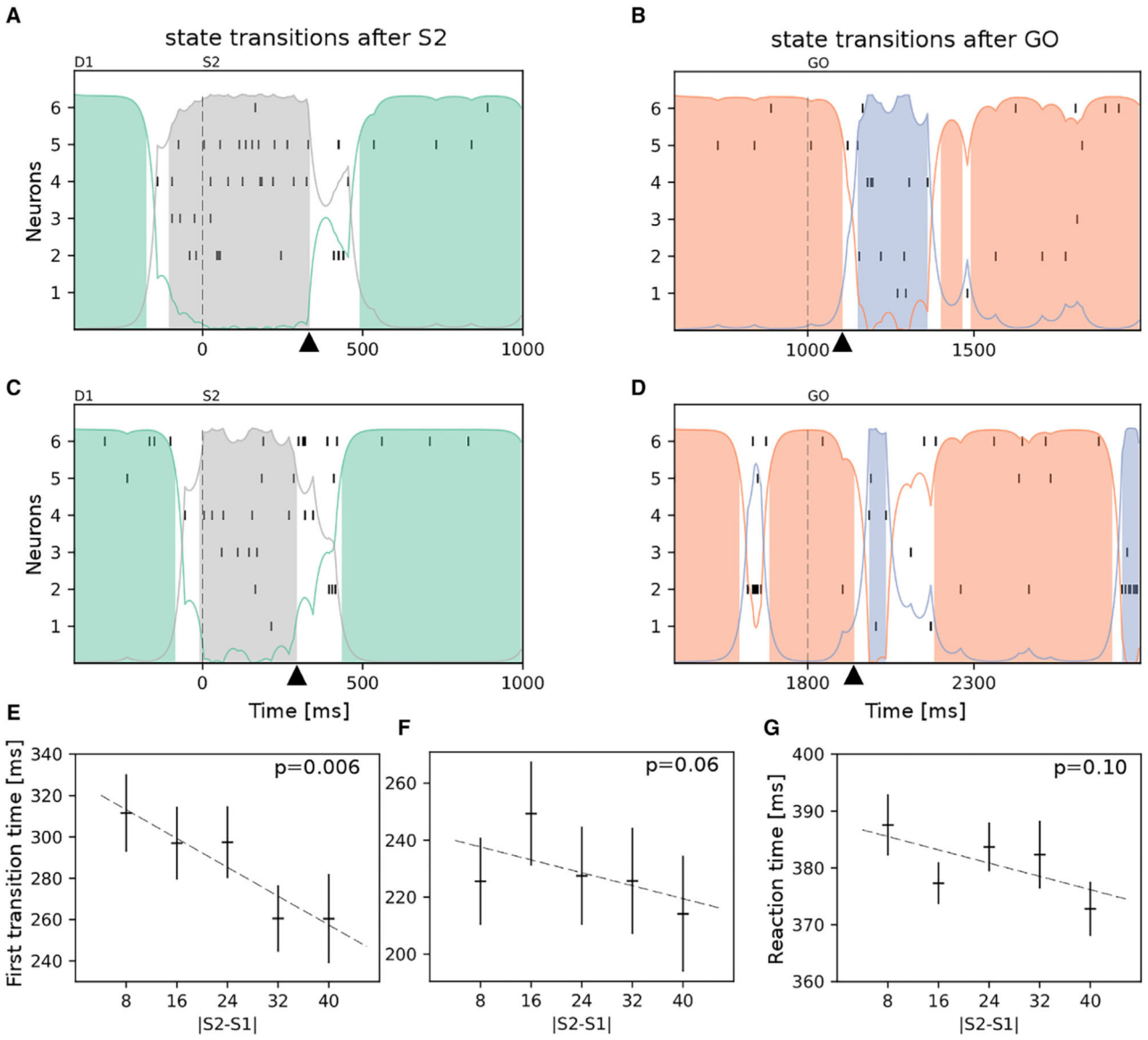

Figure 6. Analysis of first transition time after S2 (fTaS2)

(A) Example trial with rasters and HMM segmentation of a neural ensemble of 6 cells recorded simultaneously for one difficult trial, with |S2–S1| = 16. Each raster plot indicates the spiking activity of each recorded neuron from 400 ms before S2 until the end of the stimulus presentation. Same conventions as in Figure 1. The triangle on the horizontal axis marks the fTaS2. Vertical dashed line indicates S2 onset.

(B) Same trial as in (A), analyzed with an HMM around the GO signal. A time window of 1,400 ms was used: 400 ms before and 1,000 ms after the GO cue.

(C) Same as in (A), for an example of an easy trial with |S2–S1| = 40.

(D) Same as in (C), with HMM analysis around the GO signal.

(E) fTaS2 versus |S2–S1| plot (mean ± SEM) indicates a significant trend of fTaS2 with trial difficulty (p = 0.006, Jonckheere's trend test).

(F) First transition time (means ± SEM) after the GO signal versus |S2–S1|. No significant trend test, $p = 0.06$.
(G) RTs (means ± SEM) versus trial difficulty, |S2–S1|. No significant trend test, $p = 0.10$.

KEY RESOURCES TABLE

REAGENT or RESOURCE	SOURCE	IDENTIFIER
Experimental Models: Organisms/Strains		
Primate: Rhesus monkeys (Macaca mulatta)	National Institute of Mental Health, Bethesda, US	N/A
Software and Algorithms		
Multi-channel Acquisition Processor	Plexon Inc	https://plexon.com/
Off Line Sorter	Plexon Inc	https://plexon.com/
MATLAB	MathWorks	https://www.mathworks.com/
Python 2.7.0	Python Software Foundation	https://www.python.org/
In-house developed code	This paper	https://github.com/danilobenozzo/hmm_neurofis
Other		
Infrared eye-tracker system	Arrington Research, Scottsdale, USA	http://www.arringtonresearch.com/
Quartz-insulated platinum-iridium electrodes	Thomas Recording	https://www.thomasrecording.com/
Adaptive Multi-Electrode Positioning System (AMEP)	Thomas Recording	https://www.thomasrecording.com/
Neural recording data acquisition system	Plexon Inc	https://plexon.com/